Bull. Chem. Soc. Jpn., 72, 2719—2728 (1999)

Synthesis, Spectroscopy, Electrochemistry, and Mesomorphism of Triple-Decker Porphyrins Consisting of Two Cerium Ions and Three 5,15-Diarylporphyrins

Hideya Miwa, Nagao Kobayashi,* Kazue Ban,† and Kazuchika Ohta,*,†

Department of Chemistry, Graduate School of Science, Tohoku University, Sendai 980-8578

†Department of Functional Polymer Science, Faculty of Textile Science and Technology, Shinshu University, Ueda 386-8567

(Received July 13, 1999)

Triple-decker sandwich complexes, which consist of two cerium ions and three strip-like diarylporphyrins, have been synthesized and their spectroscopic and electrochemical properties and mesomorphism are reported and compared with those of the corresponding double deckers and the parent monomers. The Soret band of the triple-deckers lies at longer and shorter wavelengths than those of the double-deckers and monomers, respectively, while a sequence of small absorptions is observed in the Q band region. These are interpreted on the basis of knowledge of triple-deckers made from tetraphenylporphyrin and octaethylporphyrin. Magnetic circular dichroism (MCD) spectroscopy suggests that the Soret bands of the triple-deckers are a superimposition of at least two transitions to orbitally degenerate states. In the MCD spectra, Faraday *A*-terms are observed corresponding to each absorption band, suggesting that these triple-deckers take D_{4h} or more plausibly D_{4d} structures. Triple-deckers containing dialkoxyphenyl groups at the 5,15-positions of their parent porphyrin show a mesophase possessing both lamellar and columnar structures at lower temperatures and a columnar mesophase at higher temperatures, which differ in stacking distances. On the other hand, those containing tetraalkoxylated terphenyl groups at the 5,15-positions of their parent porphyrin show only a columnar mesophase with a single stacking distance. These differences in the mesomorphism are explained by differences of the magnitude of the steric hindrance of the side chains for rotation along the axis connecting the center of the three porphyrins.

Where is the border on molecular structures between a columnar mesogen and a calamitic (rod-like) mesogen, when the molecular shape is continuously changed from disk-like to rod-like? To resolve this question, we previously synthesized and investigated a systematic series of porphyrin derivatives substituted by various kinds of hindered groups having long flexible chains.[1] Figure 1 summarizes the relationship between the porphyrin derivative molecular type and the resulting mesophase. Type-1 disk-like $(C_{12}O)_8$tttpH$_2$ and [Cu{$(C_{12}O)_8$tttp}] derivatives having D_{4h} symmetry exhibit a typical discotic hexagonal columnar (D_h) mesophase. Type-2 strip-like derivatives $(C_nO)_8$btpH$_2$ (n = 12, 16) (**2′b**, **2′d**) having eight long chains show a discotic rectangular columnar (D_r) mesophase. On the other hand, Type-2 $(C_{12}O)_4$btpH$_2$ (**3′b**) and Type-3 $(C_nO)_4$bppH$_2$ (n = 10, 12, 14) (**1′a**, **1′b**, **1′c**) show a discotic lamellar columnar (D_{LC}) mesophase.[2] Bruce et al.[3] reported that the Type-4 rod-like porphyrin derivatives show calamitic mesophases of S_B, S_E, and $S_{E'}$ phases. As can be seen from the top derivative to the bottom one in Fig. 1, it is apparent that this kind of a successive change in molecular structure causes a change in mesophase from discotic columnar to discotic lamellar columnar, and further to calamitic.

On the other hand, there have been several reports that rod-like molecules form disk-like dimers, which exhibit discotic columnar mesophases. We previously reported that rod-like bis(*p*-*n*-alkoxy-biphenylbutane-1, 3-dionato)copper(II) complexes form disk-like dimers showing D_r mesophases.[4,5] Swager also reported that hemidisk-like molecules form pseudo disk-like dimers after rotation by 90° or 180° between neighboring discrete molecules and that they exhibit a D_h mesophase.[6] Therefore, it is interesting that even if the molecular shape is rod-like, there is still a possibility that they may exhibit discotic columnar mesophases through disk-like dimer formation.

Sandwich-type porphyrin double-decker and triple-decker metal complexes consist of two or three porphyrin macrocycles rotated by ca. 20—45° between them and stacked up by complexation. We expected that our previously reported strip-like porphyrin derivatives, **1′**, **2′**, and **3′**, might become pseudo disk-like double-decker and triple-decker derivatives through complexation.

Simon and Ohta et al. reported that long-chain-substituted bis(phthalocyaninato)lutetium double-decker derivatives show D_h mesophases and unique electrochromism[7,8] We found that the bis[octakis(dodecyloxy)phthalocyaninato]-lutetium(III) double-decker complex shows D_h mesophases and a very interesting electrical conductivity.[9]

Hence, we have synthesized various triple-decker derivatives, which consist of two rare earth metal ceriums and three

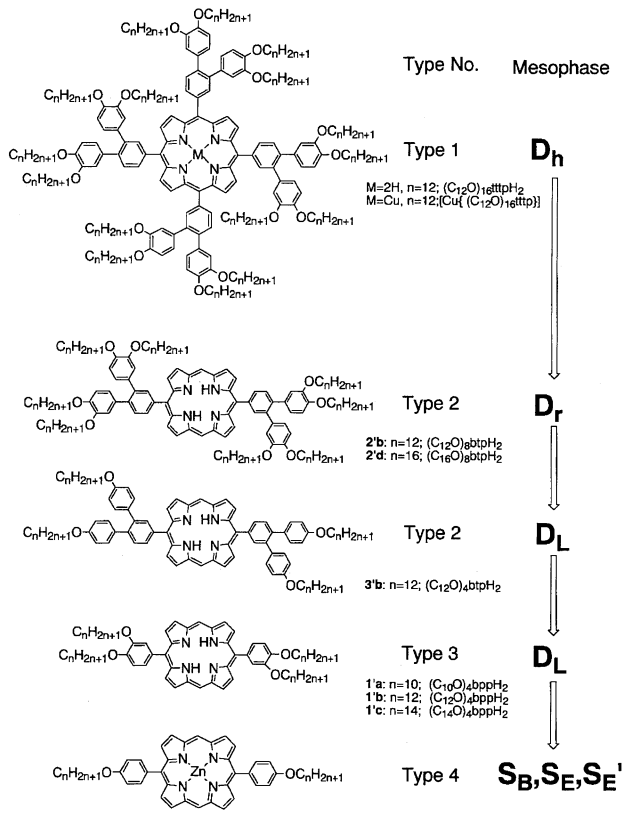

Fig. 1. The relationship between porphyrin derivatives moleculer type and the resulting mesophase.

strip-like porphyrins previously reported,[1] and investigated their mesomorphism. In addition, before measurements of the mesomorphism, their spectroscopic and electrochemical properties were examined and compared with those of the corresponding double-decker and the parent porphyrins. In this paper, the terms dimer and trimer are doubly and triply weighed aggregates in which the molecules are not actually bonded, but are associated by a molecular interaction via van der Waals forces. On the other hand, the terms double-decker and triple-decker indicate discrete molecules in which two and three components, such as porphyrin disks, are actually bonded by covalent, ionic and coordinate bonds.

Experimental

Measurements: Electronic absorption spectra were measured with a Hitachi U-3410 spectrophotometer. Magnetic circular dichroism measurements were made with a JASCO electromagnet, which gave magnetic fields up to 1.09 T with parallel and antiparallel fields. These spectroscopic measurements were performed in chloroform.

Cyclic voltammetric measurements were carried out using a Hokuto Denko HA-501 potentiostat/galvanostat connected to a Hokuto Denko HB-105 function generator. Differential pulse voltammetry experiments were performed with a Yanaco Model P-1100 electric analyzer. Conventional three-electrode cells were used, in which a glassy carbon electrode (area = 0.07 cm^2), a platinum wire and AgCl-coated Ag-wire were used as the working electrode, the auxiliary electrode and the reference electrode, respectively. These electrochemical measurements were performed in *o*-dichlorobenzene containing 0.1 M tetrabutylammonium perchlorate (TBAP) (1 M = 1 mol dm^{-3}).

The phase-transition behavior of these compounds was observed using a polarizing microscope (Olympus BH2) equipped with a heating plate controlled by a thermoregulator (Mettler FP80 hot stage, Mettler FP82 Central Processor), and measured by a differential scanning calorimeter (Shimadzu DSC-50). The X-ray diffraction measurements were performed with Cu $K\alpha$ radiation (Rigaku Geigerflex and Rigaku Rint) using a hand-made heating plate[10] controlled by a themoregulator. Temperature-dependent electronic absorption spectra were measured by a Hitachi 330 spectrophotometer equipped with a hand-made heating plate[11] controlled by a thermoregulator for the thin films of the porphyrin derivatives. These thin films were prepared by casting from a chloroform solution onto P102 glass.

Materials. The triple-decker porphyrin cerium sandwich complexes were prepared in the manner of Buchler et al.[12—14] using the corresponding diarylporphyrins, which we had previously synthesized.[1] (Fig. 2). Complexes **1a**, **1b**, and **1c** are triple-decker cerium complexes prepared from Type-3 metal-free derivatives (**1′a**, **1′b**, and **1′c**). These are abbreviated as [Ce$_2${(C$_n$O)$_4$bpp}$_3$] (n = 10, 12, 14). Complexes **2b** and **2d** (abbreviation: [Ce$_2${(C$_n$O)$_8$btp}$_3$] (n = 12, 16)) are triple-decker cerium complexes prepared from Type 2 metal-free derivatives, **2′b** and **2′d**. Complex **3b** (abbreviation: [Ce$_2${(C$_{12}$O)$_4$btp}$_3$]) is a triple-decker cerium complex obtained from a Type-4 metal-free derivative **3′b**. Table 1 summarizes the elemental-analysis data for all triple-deckers synthesized here.

Tris[5,15-bis(3,4-didodecyloxyphenyl)porphyrinato]diceri-um(III) (1b; [Ce$_2${(C$_{12}$O)$_4$bpp}$_3$]). A mixture of 5,15-bis(3,4,3″,4″-tetradodecyloxy-*o*-terphenyl)porphyrin **1′b** (59 mg, 0.049 mmol) and tris(acetylacetonato)cerium(III) (278 mg, 0.61 mmol) in 10 ml of 1,2,4-trichlorobenzene (TCB) was refluxed for 18 h. TCB was distilled under reduced pressure at 100 °C. Purification was

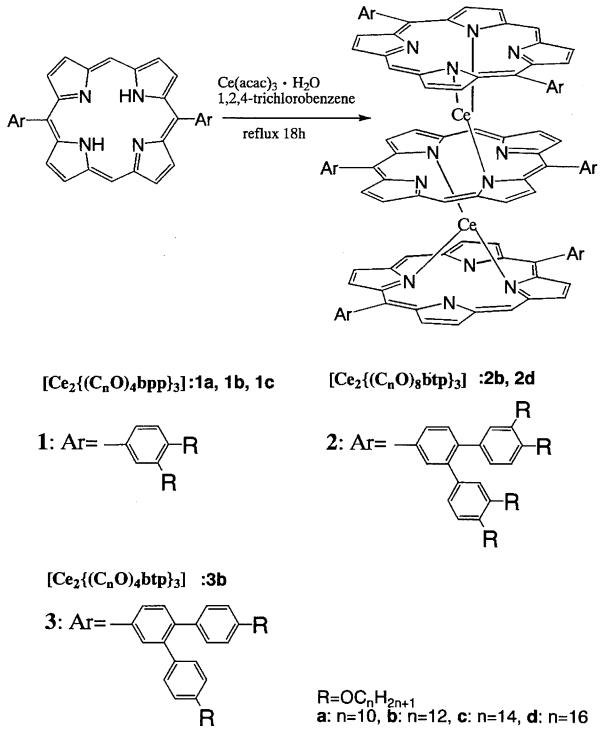

Fig. 2. Formulae of the diarylporphyrin triple-decker cerium-(III) complexes; **1a**, **1b**, **1c**, **2b**, **2d**, and **3b**.

Table 1. Elemental Analysis Data and Yields of the $[Ce_2\{(C_nO)_4bpp\}_3]$ (n = 10, 12, 14) and $[Ce_2\{(C_nO)_mbtp\}_3]$ (n = 12, 16, m = 4, 8) Derivatives

Compound	Yield	Molecular formula	Found % (Calcd %)		
	%	(Molecular weight)	C	H	N
1a: $[Ce_2\{(C_{10}O)_4bpp\}_3]$	47	$C_{216}H_{300}N_{12}O_{12}Ce_2$ (3537.09)	73.32 (73.35)	8.15 (8.55)	4.75 (4.75)
1b: $[Ce_2\{(C_{12}O)_4bpp\}_3]$	43	$C_{240}H_{348}N_{12}O_{12}Ce_2$ (3873.73)	74.32 (74.42)	9.10 (9.06)	4.22 (4.34)
1c: $[Ce_2\{(C_{14}O)_4bpp\}_3]$	38	$C_{264}H_{396}N_{12}O_{12}Ce_2$ (4210.35)	75.30 (75.31)	9.18 (9.48)	4.02 (3.99)
2b: $[Ce_2\{(C_{12}O)_8btp\}_3]$	87	$C_{456}H_{684}N_{12}O_{24}Ce_2$ (6998.80)	78.35 (78.26)	9.81 (9.85)	2.37 (2.40)
2d: $[Ce_2\{(C_{16}O)_8btp\}_3]$	81	$C_{552}H_{876}N_{12}O_{24}Ce_2$ (8345.39)	80.32 (79.45)	10.43 (10.58)	2.18 (2.01)
3b: $[Ce_2\{(C_{12}O)_4btp\}_3]$	40	$C_{312}H_{396}N_{12}O_{12}Ce_2$ (4786.91)	79.39 (78.28)	8.45 (8.34)	3.52 (3.51)

carried out using column chromatography (neutral alumina; activity III, chloroform), giving a mixture of the triple-decker, double-decker and metal-free porphyrin derivatives obtained by this column chromatography. These were then separated by gel-permeation chromatography (Bio-beads SX-1, chloroform). In the chromatography, elution occurred in the order of triple-decker, duble-decker, and metal-free derivatives. The purity of the fractions was confirmed by electronic absorption spectroscopy. After removal of the solvent, the product was further purified by reprecipitation (CH_2Cl_2 and acetone) to afford 27 mg (yield 43%) of dark-brown powder. *m/z* (FAB-MS): 3875 ($[M+1]^+$) for $[Ce_2\{(C_{12}O)_4bpp\}_3]$. The corresponding double-decker, $[Ce\{(C_{12}O)_4bpp\}_2]$, was also obtained (11 mg) and showed a peak at 2535 ($[M+1]^+$) in its FAB mass spectrum.

Other diarylporphyrin triple-decker complexes (**1a**, **1c**, **2b**, **2d**, and **3d**) were prepared in the same manner.

Results and Discussion

Electric Absorption and Magnetic Circular Dichroism Spectroscopy: Table 2 summarizes the electronic absorption spectral data for the main peaks of all triple-deckers. Figure 3 shows the electronic absorption and magnetic circular dichroism (MCD) spectra of $[Ce_2\{(C_{12}O)_4bpp\}_3]$, and also the electronic absorption spectra of $[Ce\{(C_{12}O)_4bpp\}_2]$ and $(C_{12}O)_4bppH_2$ for comparison. The Soret band of $[Ce_2\{(C_{12}O)_4bpp\}_3]$ appears at about 10 nm to a shorter or longer wavelength than that of $(C_{12}O)_4bppH_2$ or $[Ce\{(C_{12}O)_4bpp\}_2]$, respectively. The Soret bandwidth of the triple-decker is narrower than that of the double-decker, but its absorption coefficient is larger than for the latter. Moreover, in the Q band region, the spectra of $[Ce_2\{(C_{12}O)_4bpp\}_3]$ and $[Ce\{(C_{12}O)_4bpp\}_2]$ contain weak bands not seen in the spectrum of $(C_{12}O)_4bppH_2$, which are observed in the regions between the Q and Soret bands (450—500 nm) and to the red of the Q bands (630—800 nm). These feartures are similar to those reported for octaethylporphyrin triple-decker, double-decker, and tetraphenylporphyrin double-decker cerium complexes ($[Ce_2(oep)_3]$, $[Ce(oep)_2]$, and $[Ce(tpp)_2]$).[13,14] Using an exciton theory, Holten et al. explained that the blue-shift of the Soret bands of triple- and double-deckers compared with those of metal-free porphyrins is due to the face-to-face stacking of the macrocycles.[15,16] They also found that the bands at around 450—500 nm, denoted as Q″ bands, were due to charge resonance (CR) states formed by in-phase combinations of the intramolecular charge transfer, and the bands at around 630—800 nm, which were named as Q′ bands, were due to mixing between exciton and CR character.[15,16] The MCD spectrum of $[Ce_2\{(C_{12}O)_4bpp\}_3]$ is very complicated, par-

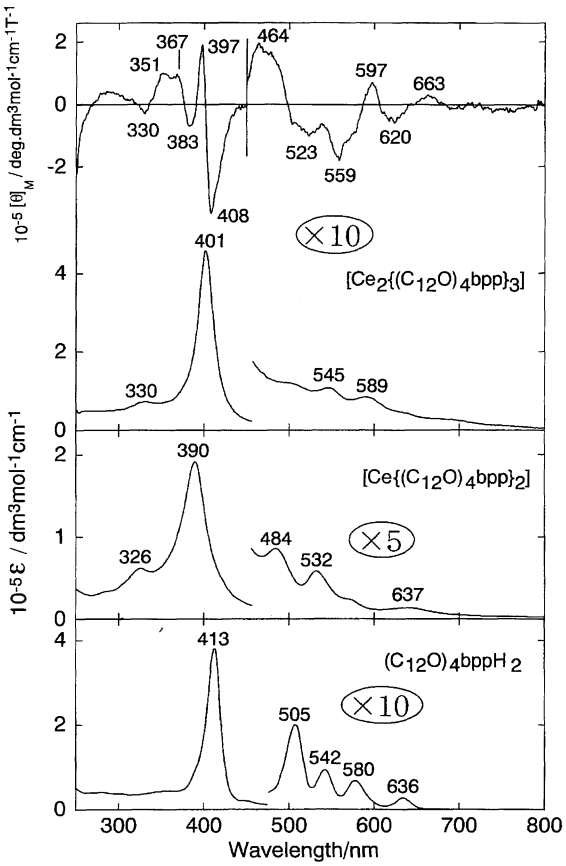

Fig. 3. Electronic absorption (and partly magnetic circular dichroism) spectra of $(C_{12}O)_4bppH_2$, $[Ce\{(C_{12}O)_4bpp\}_2]$, and $[Ce_2\{(C_{12}O)_4bpp\}_3]$ in chloroform. The applied magnetic field was 1.09 T.

Table 2. Electronic Absorption Spectral Data of the $[Ce_2\{(C_nO)_4bpp\}_3]$ (n = 10, 12, 14) and $[Ce_2\{(C_nO)_mbtp\}_3]$ (n = 12, 16, m = 4, 8) Derivatives in Chloroform

Compound	λ_{max}/nm (log ε)				
	Soret-band	Q″-band	Q-band		Q′-band
1a: $[Ce_2\{(C_{10}O)_4bpp\}_3]$	401 (5.57)	ca. 490	547 (3.99)	590 (3.88)	630—800
1b: $[Ce_2\{(C_{12}O)_4bpp\}_3]$	402 (5.76)	ca. 490	541 (4.03)	583 (3.87)	630—800
1c: $[Ce_2\{(C_{14}O)_4bpp\}_3]$	400 (5.69)	ca. 490	547 (4.03)	591 (3.93)	630—800
2b: $[Ce_2\{(C_{12}O)_8btp\}_3]$	401 (5.64)	ca. 490	538 (4.14)	575 (3.90)	630—800
2d: $[Ce_2\{(C_{16}O)_8btp\}_3]$	400 (5.61)	ca. 490	536 (4.29)	579 (4.12)	630—800
3b: $[Ce_2\{(C_{12}O)_4btp\}_3]$	401 (5.79)	ca. 490	545 (4.14)	588 (4.09)	630—800

ticularly in the Q band region, compared with those of other porphyrin monomers and $[Ce(oep)_2]$.[17,18] However, we can see at least two derivative-shaped curves (Faraday A-terms) corresponding to the main Soret absorption peak at 401 nm, suggesting that the single absorption band is actually a superimposion of at least two bands which correspond to transitions to two essentially degenerate states. Similar features have also been seen in $[Ce(oep)_2]$[18] and $[Ce\{(C_{12}O)_4bpp\}_2]$ (not shown). The interpretation in the Q band region is more complex, due to an increase in the number of absorption peaks. However, in this case also, the MCD curves appear to be composed mainly of Faraday A-terms. For example, small A-terms are seen corresponding to the absorption peaks at 545 and 589 nm. Thus, most of the bands in Fig. 3 appear to correspond to transitions to orbitally degenerate excited states. These considerations hold at least theoretically when the triple- (accordingly double- also) deckers take either D_{4d} or D_{4h} symmetry. Judging from the large size of the substituent groups, compounds **2b**, **2d**, and **3b** tend to take a D_{4d} conformation.

Electrochemistry: Figure 4 shows cyclic voltammograms of $[Ce_2\{(C_{14}O)_4bpp\}_3]$, together with those of $[Ce\{(C_{14}O)_4bpp\}_2]$ and $(C_{14}O)_4bppH_2$ for comparison. Some electrochemical data are summarized in Table 3. Two reduction and two oxidation couples were observed for $[Ce\{(C_{14}O)_4bpp\}_2]$ and $(C_{14}O)_4bppH_2$, while three reduction and two oxidation couples were seen for $[Ce_2\{(C_{14}O)_4bpp\}_3]$. In the case of the $(C_{14}O)_4bppH_2$ monomer, all redox couples are assigned to ligand oxidation or reduction. The first oxidation couple is reversible if the potential sweep is switched before reaching the second oxidation. The potential difference, ΔE, between the first oxidation and reduction potentials is 2.29 V, which is typical of those for porphyrin monomers.[19] On the other hand, as found for $[Ce(oep)_2]$ and $[Ce(tpp)_2]$,[14,20] the first reduction couple of $[Ce\{(C_{14}O)_4bpp\}_2]$ can be assigned as a metal-centered reduction. The first oxidation potential of this double-decker is more cathodic than that of $(C_{14}O)_4bppH_2$, reflecting the effect of the strong π–π interaction between the two porphyrin ligands and perhaps the presence of the Ce atom.

In the case of $[Ce_2(oep)_3]$, six oxidation and one reduction couples have been reported, and the third and fourth oxidation waves (0.80 and 0.95 V vs. Ag/AgCl) are assigned as metal-centered oxidations.[21] Hence, metal-centered oxidations can also occur in $[Ce_2\{(C_{14}O)_4bpp\}_3]$. We

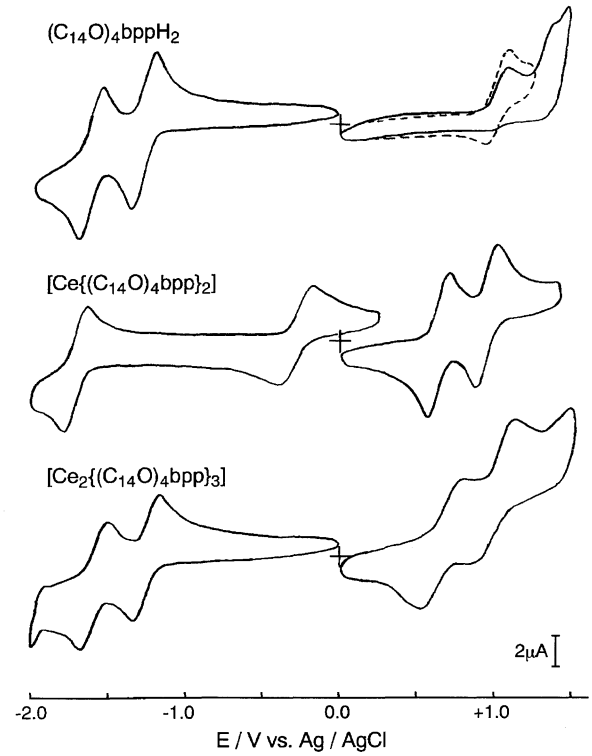

Fig. 4. Cyclic voltammograms of $(C_{14}O)_4bppH_2$, $[Ce\{(C_{14}O)_4bpp\}_2]$, and $[Ce_2\{(C_{14}O)_4bpp\}_3]$ in o-dichlorobenzene with 0.1 M TBAP. Concentrations and scan rates of all compounds are 1 mM and 50 mV s^{-1}, respectively.

attempted to confirm the origins of the oxidation couples of $[Ce_2\{(C_{14}O)_4bpp\}_3]$ by spectroelectrochemistry using an optically transparent thin-layer electrochemical cell containing a platinum wire minigrid as the working electrode. However, the triple-decker decomposed in-situ at the potential required to obtain the first oxidation product. Nevertheless, from the ΔE values (1.86 and 1.89 V for $[Ce_2(oep)_3]$[21] and $[Ce_2\{(C_{14}O)_4bpp\}_3]$, respectively), the first oxidation couple of $[Ce_2\{(C_{14}O)_4bpp\}_3]$ may be assigned as ligand-centered.

The diffusion coefficient, D, decreased from 1.55×10^{-6} $cm^2\,s^{-1}$ for $(C_{14}O)_4bppH_2$ to 1.10×10^{-6} $cm^2\,s^{-1}$ for $[Ce\{(C_{14}O)_4bpp\}_2]$ and further to 0.99×10^{-6} $cm^2\,s^{-1}$ for $[Ce_2\{(C_{14}O)_4bpp\}_3]$, reflecting their molecular size. The value for $(C_{14}O)_4bppH_2$ is slightly smaller than those reported for porphyrin[22] and phthalocyanine[23] monomers (ca. 2×10^{-6} $cm^2\,s^{-1}$), possibly due to the attached four long

Table 3. Redox Potential Data (vs. Ag/AgCl) for $(C_{14}O)_4bppH_2$, $[Ce\{(C_{14}O)_4bpp\}_2]$, and $[Ce_2\{(C_{14}O)_4bpp\}_3]$ in *o*-Dichlorobenzene Containing 0.1 M TBAP[a)]

Species	$E^{2+/1+}$	$E^{1+/0}$	$E^{0/1-}$	$E^{1-/2-}$	$E^{2-/3-}$	D / cm^2s^{-1} [d)]
$(C_{14}O)_4bppH_2$	1.32[b)]	1.01 (0.14)	−1.28 (0.17)	−1.62 (0.16)		1.55×10^{-6} [e)]
$[Ce\{(C_{14}O)_4bpp\}_2]$	0.96 (0.15)	0.64 (0.15)	−0.29 (0.19)	−1.71 (0.16)		1.10×10^{-6} [f)]
$[Ce_2\{(C_{14}O)_4bpp\}_3]$	0.99 (0.20)	0.63 (0.20)	−1.26 (0.15)	−1.60 (0.15)	−1.94[c)]	0.99×10^{-6} [g)]

a) Numbers in parentheses indicate the potential differences, ΔE_p, between cathodic and anodic peak potentials at a sweep rate 50 mV s^{-1}. b) Irreversible wave due to the chemical instability of the electrogenerated species. c) The potential was not clear in the cyclic voltammogram due to solvent cut-off, therefore, this potential was determined from a differential pulse voltammogram. d) diffusion coefficient. e) An average value determined from the current peaks at the first and second reduction waves and the first oxidation wave. f) An average value determined from all redox waves. g) An average value determined from the current peaks at the first and second reduction waves.

alkyl chains.

Mesomorphism: (1) $[Ce_2\{(C_nO)_4bpp\}_3]$ (n = 10, 12, 14). Table 4 summarizes the phase-transition temperatures and enthalpy changes for $[Ce_2\{(C_nO)_4bpp\}_3]$ (n = 10, 12, 14). The $[Ce_2\{(C_{10}O)_4bpp\}_3]$ (**1a**) complex is in a liquid-crystalline state at room temperature. When heated at 10 °C $min.^{-1}$, a small broad peak corresponding to a change from the discotic lamellar columnar (D_{LC}) mesophase to the discotic rectangular columnar (D_r) mesophase was observed at 104 °C. Upon further heating, a comparatively large peak appeared at 148 °C, which corresponds to clearing from the D_r mesophase to an isotropic liquid (I.L.). When the I.L. was cooled to room temperature by air blowing and then heated up again from r.t., it did not give the endothermic peak at 104 °C: on further heating, the phase transition from the D_r mesophase to I.L. appeared again at 148 °C. Thus, the lower temperature mesophase D_{LC} only appears in a virgin sample.

To identify these two mesophases of **1a**, temperature-dependent X-ray diffraction measurements and microscopic observations of the textures were carried out. The lower temperature mesophase was identified by X-ray diffraction for a virgin sample at 50 °C, giving four sharp reflections at the low-angle region, as summarized in Table 5. The spacings are in the ratio of 1 : 1/2 : 1/3 : 1/4, which corresponds to a lamellar structure. The X-ray pattern also has a broad peak at around 2θ = 20°, corresponding to melting of the alkyl chains. Additionally, a relatively broad peak could be observed at ca. 3.6 Å (h_1), which agreed with a stacking distance of 3.2—3.5 Å between the porphyrin monomers in a columnar structure. Moreover, two peaks could be also observed at ca. 7.9 Å (h_2) and 10.4 Å (h_3), which are very close to two and three times 3.6 Å (h_1), respectively. This suggests that these indicate the stacking distances between double-deckers (h_2) and triple-deckers (h_3). It is noteworthy that irrespective of the actual formation of triple-deckers for $[(C_{10}O)_4BPP]_3Ce_2$ (**1a**), these stacking distances between single-deckers (h_1) and double-deckers (h_2) appeared in the X-ray diffraction pattern. From a X-ray analysis, the lower temperature mesophase could be identified as a discotic lamellar columnar (D_{LC}) mesophase.

The higher temperature mesophase was identified from the X-ray diffraction pattern obtained at 130 °C. As listed in Table 5, this gave six sharp reflections in the low-angle region, indicating that this mesophase could be a discotic rectangular columnar (D_r). A further analysis from the extinction rules for two-dimensional rectangular lattices showed it to be D_r ($P2/a$). Additionally, the X-ray pattern gave a broad peak corresponding to the melting of alkyl chains and three peaks

Table 4. Phase Transition Temperatures and Enthalpy Changes of the $[Ce_2\{(C_nO)_mbtp\}_3]$ and $[Ce_2\{(C_nO)_4bpp\}_3]$ Derivatives

Complex	Phase	T (°C)[ΔH (kJ mol^{-1})]	Phase		
1a: $[Ce_2\{(C_{10}O)_4bpp\}_3]$	D_{LC}	104 [19.4] →	D_r ($P2/a$)	148 [28.9] ⇄	I.L.
1b: $[Ce_2\{(C_{12}O)_4bpp\}_3]$	D_{LC}	100 [44.5] →	D_r ($P2/a$)	143 [47.8] ⇄	I.L.
	X	← −3.2 [33.7]			
1c: $[Ce_2\{(C_{14}O)_4bpp\}_3]$	D_{LC}	106 [82.5] →	D_r ($P2/a$)	136 [42.6] ⇄	I.L.
2b: $[Ce_2\{(C_{12}O)_8btp\}_3]$	Glassy D_h	Tg=104 →	D_h	158 [12.8] ⇄	I.L.
2d: $[Ce_2\{(C_{16}O)_8btp\}_3]$	D_{h1}	49 [380] →	D_{h2}	127 [9.17] ⇄	I.L.
	X	← 27 [256]			
3b: $[Ce_2\{(C_{12}O)_4btp\}_3]$	Glassy liquid	T_g = 98 ⇄			I.L.

Phase nomenclature: D_{LC} = discotic lamellar columnar mesophase, D_r = discotic rectangular columnar mesophase, D_h = discotic hexagonal columnar mesophase, X = unidentified phase and I.L. = isotropic liquid.

Table 5. X-Ray Data of the $[Ce_2\{(C_nO)_4bpp\}_3]$ and $[Ce_2\{(C_nO)_mbtp\}_3]$ Derivatives

Complex	Mesophase {Lattice constant (Å)}	Spacing (Å) Obsd	Spacing (Å) Calcd	Miller indices (*hkl*)
1a: $[Ce_2\{(C_{10}O)_4bpp\}_3]$	D_{LC} at 50 °C	38.5	40.1	(001)
		20.3	20.0	(002)
		13.3	13.4	(003)
	c = 40.1	10.4	10.1	(004)+h_3
	h_3 = 10.4	ca. 7.9	—	h_2
	h_2 = ca. 7.9	ca. 4.2	—	a)
	h_1 = ca. 3.6	ca. 3.6	—	h_1
	$D_r(P2/a)$ at 130 °C	33.6	34.6	(100)
		29.5	29.3	(020)
		22.3	22.4	(120)
		17.2	17.0	(130)
	a = 34.6	11.5	11.5	(300)
	b = 58.6	10.7	10.7	h_3
	h_3 = 10.7	8.75	8.65	(400)
	h_2 = ca. 7.2	ca. 7.2	—	h_2
	h_1 = ca. 3.7	ca. 4.2	—	a)
		ca. 3.7	—	h_3
1b: $[Ce_2\{(C_{12}O)_4bpp\}_3]$	D_{LC} at r. t.	45.8	46.0	(001)
		22.8	22.0	(002)
		15.4	15.4	(003)
	c = 46.0	10.7	—	h_3
	h_3 = 10.7	9.25	9.48	(004)
	h_2 = ca. 6.6	ca. 6.6	—	h_2
	h_1 = 3.60	ca. 4.2	—	a)
		3.60	—	h_1
	$D_r(P2/a)$ at 140 °C	38.2	38.2	(100)
		30.4	30.4	(020)
		19.4	19.1	(200)
		16.4	16.2	(220)
		15.1	15.2	(040)
	a = 38.2	14.2	14.1	(140)
	b = 60.9	12.9	12.7	(300)
	h_3 = 10.9	10.9	10.8	(330)+h_3
	h_2 = 7.00	10.1	10.1	(060)
	h_1 = ca. 3.6	8.95	8.96	(260)
		8.42	8.47	(170)
		7.76	7.63	(500)
		7.00	—	(460)+h_2
		ca. 4.3	—	a)
		ca. 3.6	—	h_1
1c: $[Ce_2\{(C_{14}O)_4bpp\}_3]$	D_{LC} at 50 °C	24.9	25.4	(002)
		17.0	17.0	(003)
		12.7	12.7	(004)
	c = 50.4	10.2	10.2	(005)+h_3
	h_3 = 10.2	8.62	8.48	(006)
	h_2 = 7.38	7.38	7.27	(007)+h_2
	h_1 = 3.54	6.31	6.35	(008)
		4.23	—	a,b)
		3.54	—	h_1
	$D_r(P2/a)$ at 125 °C	40.0	41.1	(100)
		30.6	30.6	(020)
		20.5	20.5	(200)

a) Halo of the molten alkoxy chains. b) Not broad but fairly sharp.

Table 5. (Continued)

Complex	Mesophase {Lattice constant (Å)}	Spacing (Å) Obsd	Spacing (Å) Calcd	Miller indices (*hkl*)
	a = 41.1, b = 61.2, h_3 = 10.6, h_2 = ca. 7.1, h_1 = ca. 3.6	13.9	13.7	(300)
		10.6	10.5	(250)+h_3
		ca. 7.1	—	h_2
		ca. 4.3	—	a)
		ca. 3.6	—	h_1
2b: $[Ce_2\{(C_{12}O)_8btp\}_3]$	Glassy D_h	35.6	35.6	(100)
	at r.t.	20.4	20.6	(110)
	a = 41.1, h = ca. 9.4	ca. 9.4	—	h
		ca. 4.4	—	a)
	D_h	33.2	33.2	(100)
	at 140 °C	20.0	19.2	(110)
	a = 38.4, h = ca. 9.0	ca. 0.9	—	h
		ca. 4.6	—	a)
2d: $[Ce_2\{(C_{16}O)_8btp\}_3]$	D_{h1}	38.8	38.8	(100)
	at r.t.	22.2	22.4	(110)
	a = 44.8, h = ca. 9.2	ca. 9.2	—	h
		4.16	—	a,b)
	D_{h2}	37.6	37.6	(100)
	at 120 °C	21.9	21.7	(110)
	a = 43.4, h = ca. 9.6	ca. 9.6	—	h
		ca. 4.6	—	a)

at 10.7 Å (h_3), ca. 7.2 Å (h_2) and ca. 3.7 Å (h_1) corresponding to the stacking distances between triple-deckers, double-deckers, and single-deckers, respectively, as well as the lower temperature mesophase. Later, this will be discussed again together with the results of electronic absorption spectra of thin films.

The $[Ce_2\{(C_{12}O)_4bpp\}_3]$ (**1b**) and $[Ce_2\{(C_{14}O)_4bpp\}_3]$ (**1c**) derivatives with different lengths of alkoxy chains show almost the same phase transition behavior as the $[Ce_2\{(C_{10}O)_4bpp\}_3]$ (**1a**) homologue (Table 4). Exceptionally, the $[Ce_2\{(C_{12}O)_4bpp\}_3]$ (**1b**) derivative has an additional phase X. When this derivative (**1b**) was cooled at −10 °C min^{-1} to −50 °C and then heated at 10 °C min^{-1}, it gave a broad endothermic peak at −32 °C, which corresponds to a phase transition from the X phase to the D_r mesophase. The X phase could not be identified within the instrumental limits because it exists only at low temperature.

Now, the present mesomorphism will be compared with that of the corresponding metal-free derivatives, $(C_nO)_4bppH_2$ (n = 10, 12, 14) (**1′a**, **1′b**, **1′c**). Each of the metal-free derivatives (**1′a**, **1′b**, **1′c**) exhibits a D_{LC} mesophase, as previously reported.[1,2] On the other hand, each of the corresponding triple-decker cerium complexes exhibits a D_{LC} mesophase at lower temperatures, but a $D_r(P2/a)$ mesophase at higher temperatures. Thus, according to our expectation, a stack of three strip-like metal-free diarylporphyrins could form a pseudo-disk, to give a columnar mesophase.

$[Ce_2\{(C_nO)_mbtp\}_3]$ (n = 12, 16; m = 4, 8). The phase-transition temperatures and enthalpy changes for the $[Ce_2\{(C_nO)_mbtp\}_3]$ (n = 12, 16; m = 4, 8) derivatives are listed in Table 4. When the $[Ce_2\{(C_{12}O)_4btp\}_3]$ (**3b**) derivative was heated at 10 °C min^{-1}, a glass transition was observed at ca. 98 °C by a DSC measurement. Upon further heating to 250 °C, no transitions were seen. Upon cooling down by air blowing to room temperature and then heating up at 10 °C min^{-1}, the material showed only a glass transition at ca. 100 °C. When viewed by a polarizing microscope, it was rigid and showed no birefringence from r.t. to ca. 100 °C. Above 100 °C, however, it became an isotropic liquid. Hence, it can be concluded that this derivative (**3b**) is a glassy liquid at r.t. and an isotropic liquid above the glass transition point.

When the $[Ce_2\{(C_{12}O)_8btp\}_3]$ (**2b**) derivative was heated from −50 °C at 10 °C min^{-1}, a glass transition from a glassy D_h mesophase to a D_h mesophase could be detected at 104 °C by a DSC measurement. Upon further heating, a relatively small endothermic peak occured at 158 °C, corresponding to clearing from the D_h mesophase to an isotropic liquid. When this I.L. was cooled to −50 °C at −10 °C min^{-1} and then heated again at 10 °C min^{-1}, it again showed a clearing endothermic peak at 158 °C. Identification of the mesophase was achieved by X-ray diffraction measurements at r.t. and 140 °C (data summarized in Table 5). The glassy mesophase at r.t. gave two sharp peaks in the low angle-region, with spacings in a ratio of $1:\sqrt{3}$. Hence, the glassy mesophase could be identified as a glassy D_h mesophase. Additionally, there was a broad peak at ca. 9.0 Å due to the stacking distance between the triple-deckers. The mesophase at 140 °C also gave two sharp peaks in the low angle region, with spacings in a ratio of $1:1/\sqrt{3}$. Hence, this mesophase was also identified as D_h. Additionally, a broad peak occurred at ca. 9.0 Å due to the stacking distance between the triple-deckers. As shown in Fig. 5, this phase showed a fan-shaped

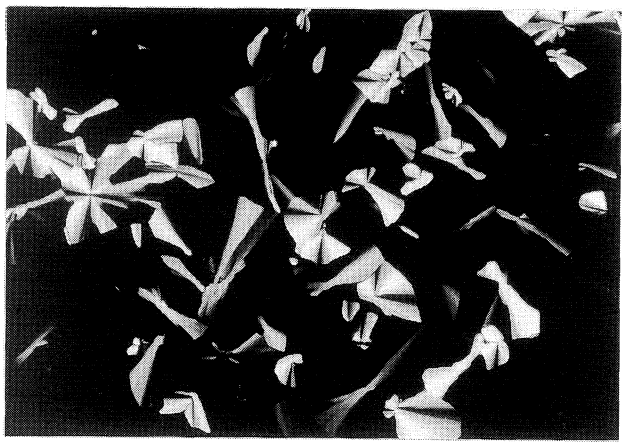

Fig. 5. Photomicrograph of the D_h mesophase of $[Ce_2\{(C_{12}O)_8btp\}_3]$ (**2b**) at 155 °C.

texture typical of a D_h mesophase. This is compatible with the X-ray results.

The $[Ce_2\{(C_{16}O)_8btp\}_3]$ (**2d**) derivative shows a mesophase at r.t. (Table 4). When it was heated from r.t. at 10 °C min^{-1}, a large endothermic peak corresponding a phase transition from a D_{h1} mesophase to a D_{h2} mesophase at 49 °C could be observed by a DSC measurement; upon further heating, a small endothermic peak due to clearing from D_{h2} to an isotropic liquid at 127 °C was detected. When the I.L. was cooled to −50 °C at −10 °C min^{-1} and then heated, a large, new endothermic peak appeared at 27 °C. This is due to a phase transition from an unidentified phase X to the D_{h2} mesophase. Upon further heating, a small peak due to clearing from I.L. to D_{h2} appeared again at 127 °C. Thus, the non-virgin sample of **2d** showed an X phase which could not be observed in the virgin sample. These mesophases were established by X-ray diffraction measurements at r.t. and 120 °C (Table 5). However, it was impossible to identify the X phase which appeared only for a non-virgin sample, because this phase gradually changed during the X-ray diffraction measurement at r.t. The virgin sample at r.t. gave two sharp peaks in the low angle region, with spacings in a ratio of $1 : 1/\sqrt{3}$. Hence, this phase could be identified as a D_h mesophase. Additionally, it gave a broad peak at ca. 9.2 Å due to the stacking distance between the triple-deckers. The higher temperature mesophase also gave two sharp peaks in the low angle region with spacing in the ratio of $1 : 1/\sqrt{3}$, and a broad peak at ca. 9.6 Å due to the stacking distance between the triple-deckers. This derivative (**2d**) exhibits two very similar D_h mesophases. To distinguish these, the lower and higher temperature D_h mesophases are named as D_{h1} and D_{h2}, respectively, for convenience in this paper. Since the hexagonal lattice constants are a = 44.8 Å for D_{h1} and a = 43.4 Å for D_{h2}, there is no great difference. Nevertheless, the mesophase-mesophase transition showed a very large endothermic peak of 380 kJ mol^{-1}, as mentioned above. The difference between these two D_h mesophases is not clear at present.

As reported previously, each of the corresponding metal-free derivatives $(C_nO)_8btpH_2$ (n = 12, 16) (**2′b** and **2′d**) exhibits a D_r mesophase. In contrast to these, the present Ce complexes **2b** and **2d** exhibit D_h mesophases. This may be attributable to the formation of a pseudo-disk by the stacking of three strip-like diarylporphyrins, according to our expectation.

Precession Movement: There is a large difference between the X-ray diffraction patterns of $[Ce_2\{(C_nO)_4bpp\}_3]$ (n = 10, 12, 14) and $[Ce_2\{(C_nO)_8btp\}_3]$ (n = 12, 16) in terms of the stacking distances, as mentioned above. We now discuss two representative examples of $[Ce_2\{(C_{14}O)_4bpp\}_3]$ for $[Ce_2\{(C_nO)_4bpp\}_3]$, and $[Ce_2\{(C_{16}O)_8btp\}_3]$ for $[Ce_2\{(C_nO)_8btp\}_3]$. Figure 6 illustrates the X-ray diffraction patterns of these mesophases. The $[Ce_2\{(C_{14}O)_4bpp\}_3]$ derivative shows three peaks due to the stacking distances between triple-deckers (10.6 Å, 10.2 Å), double-deckers (ca. 7.1 Å, 7.38 Å), and single-deckers (ca. 3.6 Å, 3.54 Å) in the both mesophases. It is reasonable that both gave a relatively sharp peak at ca. 10 Å, because this complex is a triple-decker sandwich. It is very interesting that both meosphases of this complex **1c** additionally gave two relatively small, broad peaks due to the stacking distances between double-deckers (ca. 7 Å) and single-deckers (ca. 3.5 Å), suggesting that the porphyrin disks in each of the triple-deckers fluctuate and rotate to some extent. In this respect, Aida et al. reported that optically active single-handed dou-

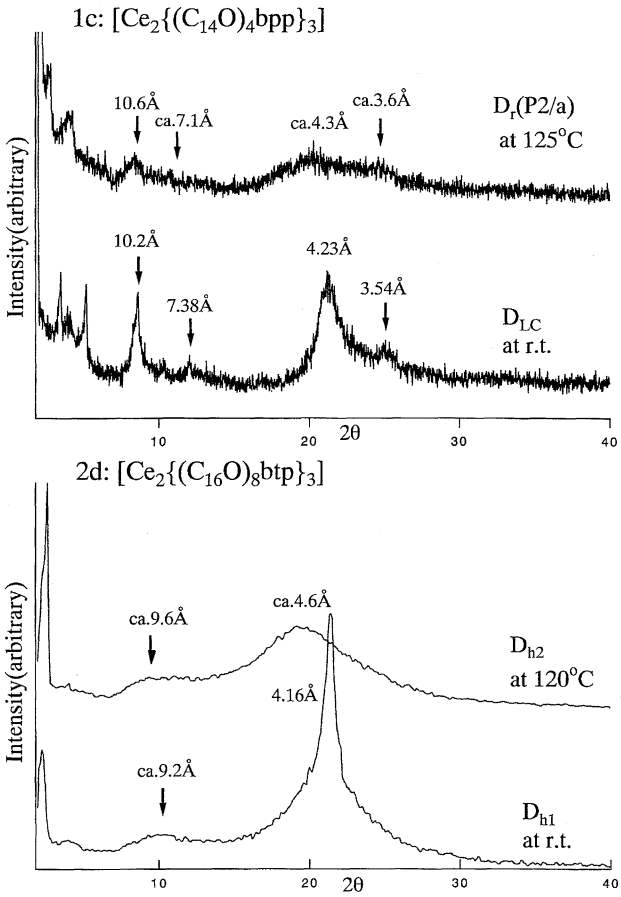

Fig. 6. X-Ray diffraction patterns of the diarylporphyrin triple-decker cerium complexes.

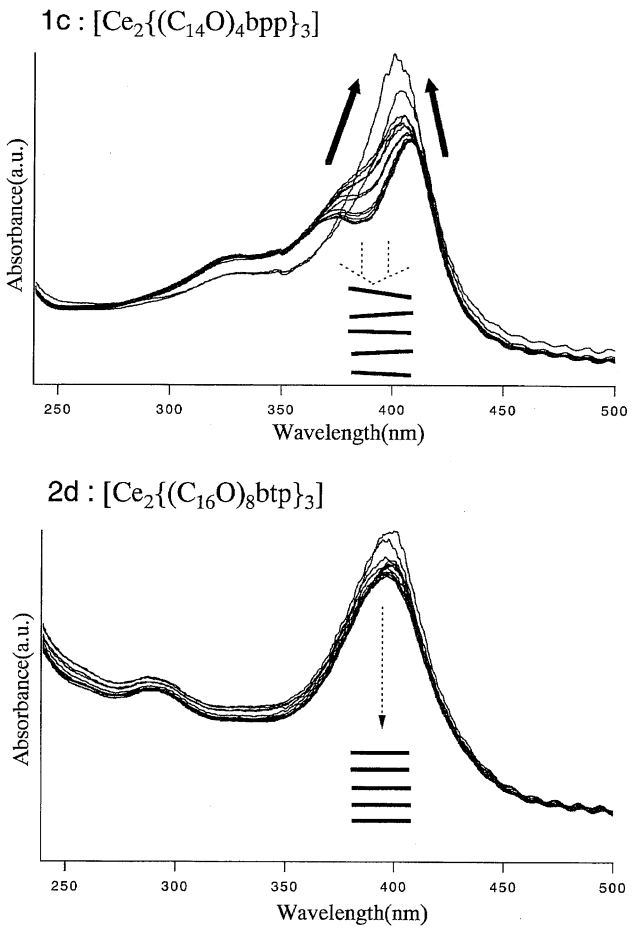

Fig. 7. Temperature-dependent electronic spectra of films of $[Ce_2\{(C_{14}O)_4bpp\}_3]$ and $[Ce_2\{(C_{16}O)_8btp\}_3]$.

ble-decker cerium porphyrins racemize in solution even at 10 °C.[24] On the other hand, the $[Ce_2\{(C_{16}O)_8btp\}_3]$ derivative gave only a stacking distance between triple-deckers at ca. 9 Å. This suggests that the porphyrin disks in each of the triple-deckers do not fluctuate and rotate, so that these triple-deckers, themselves, rotate as units, because the *o*-terphenyl groups are large enough to give steric hindrance.

To certify this hypothesis, temperature-dependent electronic absorption spectra of thin cast films of these $[Ce_2\{(C_{14}O)_4bpp\}_3]$ and $[Ce_2\{(C_{16}O)_8btp\}_3]$ derivatives were measured from r.t. to each of the clearing points at 10 °C intervals (Fig. 7). As can be seen from the upper part of Fig. 7, the spectrum of the $[Ce_2\{(C_{14}O)_4bpp\}_3]$ derivative gave two split Soret bands at r.t. It is apparent from Kasha's rule that the porphyrin planes in triple-deckers are not arranged face-to-face, but in a herringbone pattern by fluctuation. Taking into consideration the X-ray results, the porphyrin planes in triple-deckers fluctuate but do not freely rotate because these planes are connected via cerium. Hence, these porphyrin planes may show a restrictedly hindered precessional movement around the cerium pivot. With increasing temperature, the split Soret bands converge and finally become a single band in the isotropic liquid (Fig. 7). This is attributable to the more vigorous precessional movement of the porphyrin planes at higher temperatures: on the time average, these planes may be parallel.

In contrast, the $[Ce_2\{(C_{16}O)_8btp\}_3]$ derivative gave a single Soret band from r.t. to the clearing point, indicating that the porphyrin planes in triple-deckers are parallel throughout. Taking into consideration the above X-ray results, the porphyrin planes in triple-deckers do not fluctuate but are in

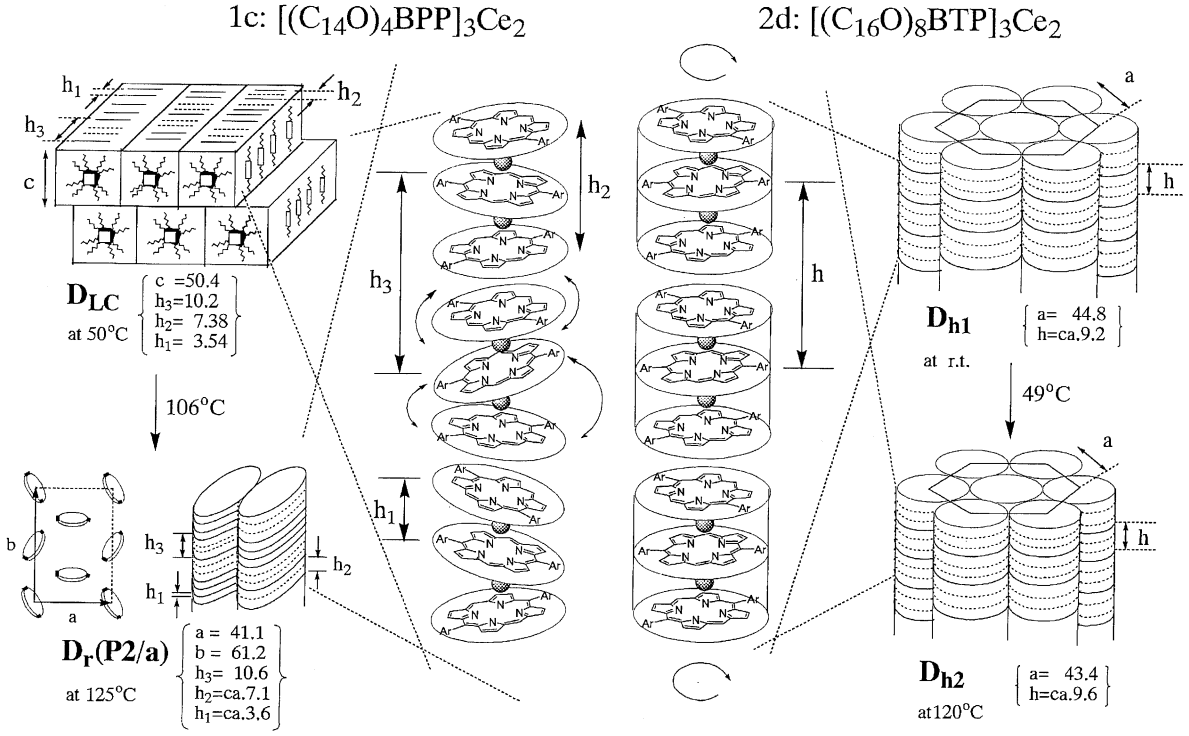

Fig. 8. Precessional movement of $[Ce_2\{(C_{14}O)_4bpp\}_3]$ and rotation of columns of $[Ce_2\{(C_{16}O)_8btp\}_3]$.

parallel: The whole triple-decker molecule rotates as a unit in the columns. The reason why the $[Ce_2\{(C_{16}O)_8btp\}_3]$ derivative does not show a similar precession movement to the $[Ce_2\{(C_{14}O)_4bpp\}_3]$ derivative is due to the bulkiness of the substituent in the porphyrin plane: being phenyl groups for $[Ce_2\{(C_{14}O)_4bpp\}_3]$ and very bulky *o*-terphenyl groups for $[Ce_2\{(C_{16}O)_8btp\}_3]$. The *o*-terphenyl groups of the neighboring disk may interact with each other to prevent the rotation, resulting in a face-to-face (parallel) arrangement of the disks in triple-deckers.

Conclusion

Triple-decker sandwich complexes (**1a**, **1b**, **1c**, **2b**, **2d**, and **3b**) consisting of two rare earth metal ceriums and three strip-like diarylporphyrins, were synthesized and their spectroscopic and electrochemical properties and mesomorphism investigated. The spectroscopic and electrochemical data resemble those of previously reported triple-decker porphyrins. MCD spectroscopy suggests that these triple-deckers take either D_{4h} or, more plausibly, D_{4d} conformation, since Faraday *A* terms were observed corresponding to most of the weak absorption peaks in the Q band region. The Soret bands of these triple-deckers consists of superimpositions of at least two transitions to the degenerate states.

Mesophases of the triple-deckers are summarized in Fig. 8. Each of the $[Ce_2\{(C_nO)_4bpp\}_3]$ (n = 10, 12, 14) derivatives (**1a**, **1b**, **1c**) having dialkoxyphenyl groups in the periphery shows a D_{LC} mesophase possessing both lamellar and columnar structures at lower temperatures, and a $D_r(P2/a)$ columnar mesophase at higher temperatures. Furthermore, each of these complexes gave three stacking distances between triple-deckers (h_3), double-deckers (h_2), and single-deckers (h_1) in the X-ray diffraction patterns. This is attributable to a fluctuation of the porphyrin planes in the triple-deckers. The temperature-dependent electronic absorption spectra of thin films revealed that the porphyrin planes are arranged in a herringbone pattern. Taking into consideration the results of X-ray diffraction studies, the porphyrin planes do not freely rotate, but show a hindered precessional movement around the cerium pivot. A more vigorous precessional movement occurs at higher temperatures; on the time average, these planes become parallel.

In contrast, each of the $[Ce_2\{(C_nO)_8btp\}_3]$ (n = 12, 16) derivatives (**2b**, **2d**) having *o*-terphenyl groups in the periphery show only D_h columnar mesophases. These complexes showed only one stacking distance between triple-deckers in the X-ray diffraction patterns, in contrast to three for **1a**, **1b**, and **1c**. Hence, the porphyrin planes in the triple-deckers **2b** and **2d** do not fluctuate and rotate. Since the temperature-dependent electronic absorption spectra show an unsplit Soret band, and since the *o*-terphenyl groups of **2b** and **2d** are very bulky, these groups of neighboring disks may bite into each other to prevent such a precessional movement. Thus, we determined the precessional movement in these triple-decker diaryl-porphyrin derivatives, and revealed that this movement is prevented by strerically hindering groups. We also found that the mesophases change from lamellar type to columnar type upon changing from the strip-like diarrylporphyrin metal-free derivatives to the corresponding pseudo disk-like cerium triple-decker complexes.

References

1 K. Ohta, N. Yamaguchi, and I. Yamamoto, *J. Mater. Chem.*, **8**, 2637 (1998).

2 K. Ohta, K. Ban, and I. Yamamoto, in preparation.

3 D. W. Bruce, D. S. Dumur, L. S. Santa, and M. A. Wali, *J. Mater. Chem.*, **2**, 363 (1992).

4 K. Ohta, O. Takenaka, H. Hasebe, Y. Morizumi, T. Fujimoto, and I. Yamamoto, *Mol. Cryst. Liq. Cryst.*, **195**, 135 (1991).

5 K. Ohta, H. Akimoto, T. Fujimoto, and I. Yamamoto, *J. Mater. Chem.*, **4**, 61 (1994).

6 A. G. Serrette, C.-K. Lai, and T. M. Swager, *Chem. Mater.*, **6**, 22552 (1994).

7 C. Piechocki and J. Simon, *Chem. Phys. Lett.*, **122**, 124 (1985).

8 T. Komatu, K. Ohta, T. Fujimoto, and I. Yamamoto, *J. Mater. Chem.*, **4**, 533 (1994).

9 A. M. van de Craats, J. M. Warman, H. Hasebe, R. Naito, and K. Ohta, *J. Phys. Chem., B*, **101**, 9224 (1997).

10 H. Ema, Master Thesis, Shinshu University, Ueda, Japan, 1988.

11 H. Hasebe, Master Thesis, Shinshu University, Ueda, Japan, 1991.

12 J. W. Buchler, H. G. Kapellmann, M. Knoff, K. L. Lay, and S. Pfeifer, *Z. Naturforsch., Teil B*, **38**, 1339 (1983).

13 J. W. Buchler, A. De Cian, J. Fischer, M. Kihn-Botulinski, H. Paulus, and R. Weiss, *J. Am. Chem. Soc.*, **108**, 3652 (1986).

14 A. De Cian, J. Fischer, P. Hammerschmidt, J. Löffler, B. Scharbert, R. Weiss, and J. W. Buchler, *Chem. Ber.*, **122**, 2219 (1989).

15 O. Bilsel, J. Rodriguez, S. N. Milan, P. A. Gorlin, G. S. Girolami, K. S. Suslick, and D. Holten, *J. Am. Chem. Soc.*, **114**, 6528 (1992).

16 L. L. Wittmer and D. Holten, *J. Phys. Chem.*, **100**, 860 (1996).

17 J. C. Sutherland, in "The Porphyrins," ed by D. Dolphin, Academic, New York (1978), Vol. III, Chap. 4.

18 S. Radzki, J. Mack, and M. J. Stillman, *New. J. Chem.*, **16**, 583 (1992).

19 D. G. Davis, in "The Porphyrins," ed by D. Dolphin, Academic, New York (1978), Vol. V, Chap. 4.

20 J. W. Buchler and B. Scharbert, *J. Am. Chem. Soc.*, **110**, 4272 (1988).

21 J. K. Duchowski and D. F. Bocian, *J. Am. Chem. Soc.*, **112**, 8807 (1990).

22 P. A. Forshey, T. Kuwana, N. Kobayashi, and T. Osa, *Am. Chem. Soc., Adv. Chem. Ser.*, **201**, 601 (1982).

23 N. Kobayashi and Y. Nishiyama, *J. Phys. Chem.*, **89**, 1167 (1985).

24 K. Tashiro, K. Konishi, and T. Aida, *Angew. Chem., Int. Ed. Engl.*, **36**, 856 (1997).